OPEN ACCESS

EXTENDED REPORT

SAMHD1 prevents autoimmunity by maintaining genome stability

Stefanie Kretschmer,[1] Christine Wolf,[1] Nadja König,[1] Wolfgang Staroske,[2] Jochen Guck,[2,3] Martin Häusler,[4] Hella Luksch,[1] Laura A Nguyen,[5] Baek Kim,[5,6] Dimitra Alexopoulou,[2,7] Andreas Dahl,[2,7] Alexander Rapp,[8] M Cristina Cardoso,[8] Anna Shevchenko,[9] Min Ae Lee-Kirsch[1]

Handling editor Tore K Kvien

▶ Additional material is published online only. To view please visit the journal online (http://dx.doi.org/10.1136/annrheumdis-2013-204845).

For numbered affiliations see end of article.

Correspondence to
Professor Min Ae Lee-Kirsch, Department of Pediatrics, Medizinische Fakultät Carl Gustav Carus, Technische Universität Dresden, Dresden, Germany, Fetscherstr 74, Dresden 01307, Germany; minae.lee-kirsch@uniklinikum-dresden.de

Received 31 October 2013
Revised 31 December 2013
Accepted 2 January 2014
Published Online First
20 January 2014

To cite: Kretschmer S, Wolf C, König N, *et al*. *Ann Rheum Dis* 2015;**74**:e17.

ABSTRACT

Objectives The HIV restriction factor, SAMHD1 (SAM domain and HD domain-containing protein 1), is a triphosphohydrolase that degrades deoxyribonucleoside triphosphates (dNTPs). Mutations in SAMHD1 cause Aicardi–Goutières syndrome (AGS), an inflammatory disorder that shares phenotypic similarity with systemic lupus erythematosus, including activation of antiviral type 1 interferon (IFN). To further define the pathomechanisms underlying autoimmunity in AGS due to SAMHD1 mutations, we investigated the physiological properties of SAMHD1.

Methods Primary patient fibroblasts were examined for dNTP levels, proliferation, senescence, cell cycle progression and DNA damage. Genome-wide transcriptional profiles were generated by RNA sequencing. Interaction of SAMHD1 with cyclin A was assessed by coimmunoprecipitation and fluorescence cross-correlation spectroscopy. Cell cycle-dependent phosphorylation of SAMHD1 was examined in synchronised HeLa cells and using recombinant SAMHD1. SAMHD1 was knocked down by RNA interference.

Results We show that increased dNTP pools due to SAMHD1 deficiency cause genome instability in fibroblasts of patients with AGS. Constitutive DNA damage signalling is associated with cell cycle delay, cellular senescence, and upregulation of IFN-stimulated genes. SAMHD1 is phosphorylated by cyclin A/cyclin-dependent kinase 1 in a cell cycle-dependent manner, and its level fluctuates during the cell cycle, with the lowest levels observed in G_1/S phase. Knockdown of SAMHD1 by RNA interference recapitulates activation of DNA damage signalling and type 1 IFN activation.

Conclusions SAMHD1 is required for genome integrity by maintaining balanced dNTP pools. dNTP imbalances due to SAMHD1 deficiency cause DNA damage, leading to intrinsic activation of IFN signalling. These findings establish a novel link between DNA damage signalling and innate immune activation in the pathogenesis of autoimmunity.

INTRODUCTION

SAMHD1 (SAM domain and HD domain-containing protein 1) functions as a dGTP-dependent triphosphohydrolase which converts deoxyribonucleoside triphosphates (dNTPs) into the constituent deoxynucleoside and inorganic triphosphate.[1 2] SAMHD1 was recently identified as the restriction factor that renders human myeloid cells non-permissive to HIV-1 infection by depleting the dNTP pool required for reverse transcription of the viral RNA genome.[3] This is counteracted by Vpx, a primate lentivirus auxiliary protein that targets SAMHD1 for proteasomal degradation.[4 5] Mutations of *SAMHD1* cause Aicardi–Goutières syndrome (AGS), an infancy-onset inflammatory encephalopathy that phenotypically mimics congenital viral infection[6] and shows overlap with systemic lupus erythematosus (SLE), a multifactorial disease characterised by autoimmunity against nucleic acids.[7] Both disorders are characterised by the formation of antinuclear antibodies and constitutive activation of antiviral type 1 interferon (IFN).[8 9] Indeed, type 1 IFN plays a central role in SLE pathogenesis by initiating a self-perpetuating feedback loop that drives autoantibody production.[9]

AGS is also caused by mutations of genes of the nucleic acid-metabolising enzymes, three prime repair exonuclease 1 (*TREX1*), ribonuclease H2 (*RNASEH2A*, *RNASEH2B*, *RNASEH2C*) and RNA-specific adenosine deaminase 1 (*ADAR1*).[10–12] While these enzymes carry out diverse functions within the intracellular nucleic acid metabolism, their deficiency is thought to result in the accrual of endogenous nucleic acid species that are recognised as danger signals by sensors of the innate immune system, which trigger the pathogenic type 1 IFN response.[13] These findings underline an important role of intracellular nucleic acid metabolism in the maintenance of immune tolerance by preventing an inadequate innate immune response induced by recognition of self nucleic acids.

Despite the antiretroviral property of SAMHD1, absence of viral infection is a cardinal feature of AGS, suggesting an intrinsic cause for activation of an innate immune response in patients with AGS. This notion is supported by the finding of a spontaneous cell-intrinsic antiviral response in SAMHD1-deficient mice.[14 15] dNTPs are the building blocks of DNA synthesis during genome replication, and their intracellular concentration requires tight control to preserve genome integrity, as imbalances in DNA precursor pools can impede DNA replication/repair leading to DNA damage, cell cycle arrest or cell death.[16] Here we provide evidence for an important role for SAMHD1 in genome stability, implicating DNA damage and/or

the cellular response to DNA damage in the pathogenesis of inflammation and autoimmunity.

METHODS

Human subjects

Primary fibroblast cell lines were derived from skin biopsy samples. The study protocol was approved by the ethics committee of the Medical Faculty, Technische Universität Dresden, and written informed consent was obtained from all patients or their parents.

Plasmids, transfection, RNA interference

Human SAMHD1 cDNA was cloned into pEGFP-C1 (green fluorescent protein (GFP)–SAMHD1) and pEGFP-N1 (SAMHD1–GFP) (Clontech). GFP was replaced by mCherry using AgeI and BsrGI. Human cyclin A cDNA was cloned into pEGFP-C1 (GFP–cyclin A). Cells were transfected with fluorescently tagged SAMHD1 or cyclin A as described.[17] For RNAi, HeLa cells were transfected with Silencer Select small interfering (si)RNAs (Ambion, see online supplementary table S1) using Oligofectamine (Invitrogen).

Cell proliferation, cell cycle analysis and β-galactosidase staining

Human fibroblasts, HeLa and HEK293T cells were cultured in Dulbecco's modified Eagle's medium containing 10% fetal bovine serum, 2 mM L-glutamine and antibiotics. In all experiments, passage-matched fibroblasts (passages 4–11) were used. Fibroblasts were seeded at a density of 2×10^5 cells/25 cm^2 flask and counted at indicated time points using a Neubauer chamber. Cells were synchronised by serum starvation for 48 h and harvested at the indicated time points after cultivation in growth medium for propidium iodide staining or lysate preparation. Flow cytometry was performed on an LSR II (Becton Dickinson), and the data were analysed using FACSDiva and FlowJo. Cells were stained using the Senescence β-Galactosidase Staining Kit (Cell Signaling). The percentage of blue cells in eight randomly chosen visual fields per slide was determined by light microscopy.

Quantitative reverse transcription (RT)-PCR

RNA was extracted with the RNeasy Mini Kit (Qiagen) followed by DNase I digestion. Target gene expression (see online supplementary table S2) was determined by quantitative RT-PCR using Taqman Universal PCR Master Mix (Applied Biosystems) on an ABI7300 and normalised to *GAPDH*.

Intracellular dNTP quantification

dNTP levels were determined by a primer extension assay as described.[18]

In vitro phosphorylation assay

Recombinant human GST-SAMHD1 was generated and purified as described.[18] SAMHD1 (15 ng) was incubated for 2 h at 30°C with recombinant cyclin A2/cyclin-dependent kinase (CDK)1, cyclin A2/CDK2 or cyclin E/CDK3 (Sigma-Aldrich) in the presence of 10 mM ATP according to the manufacturer's protocol. Kinase reactions were subjected to immunoblotting with phospho-T592-SAMHD1 antibody and SAMHD1 antibody.

Statistical analysis

Comparison of means was carried out using Student's t test. $p<0.05$ was considered significant. Data are presented as mean ±SD or mean ± SEM as indicated.

Additional methods are described in supplementary methods.

RESULTS

SAMHD1-deficient fibroblasts show impaired proliferation and cellular senescence

To investigate the consequences of SAMHD1 deficiency, we examined the cellular phenotype of primary fibroblasts from two patients with AGS both of whom presented signs of systemic autoimmunity including antinuclear antibodies, thrombocytopenia, cutaneous chilblain lesions and arthralgia.[7] Patient 1 (AGS1) was compound heterozygous for R290H and Q548X, and patient 2 (AGS2) was homozygous for H167Y, which alters one of the two highly conserved histidine residues of the catalytic HD domain.[7] We had previously shown that SAMHD1 protein is reduced or absent in AGS patient cells.[17] Consistent with this, the intracellular levels of deoxyadenosine triphosphate (dATP) and deoxythymidine triphosphate (dTTP) were at least 15-fold higher than in wild-type fibroblasts (figure 1A). Patient cells proliferated significantly more slowly than wild-type cells (figure 1B). Flow cytometry of synchronised cells demonstrated that reduced proliferation was not due to increased apoptosis, as shown by the absence of a $subG_1$ peak, but rather by a delay in cell cycle progression (figure 1C). This was accompanied by induction of the cell cycle inhibitors, p21 and p16, and an increase in β-galactosidase-positive cells, reflecting an increase in lysosomal activity consistent with cellular senescence (figure 1D,E). In addition, patient cells exhibited an enlarged and flattened morphology as well as senescence-associated heterochromatin foci within the nuclei, reflecting genome silencing (see online supplementary figure S1). These findings suggest that dysregulation of the intracellular dNTP pool due to SAMHD1 deficiency causes a cellular stress response leading to premature senescence.

DNA damage in SAMHD1-deficient cells is accompanied by type 1 IFN activation

Given the importance of balanced dNTP pools for genome stability, we examined SAMHD1-deficient cells for signs of DNA damage. We investigated the overall nuclear genome integrity by alkaline single-cell gel electrophoresis or comet assay, which detects alkali-labile sites such as single DNA strand breaks, abasic sites or incomplete excision repair sites, as well as stalled replication forks. In the absence of exogenous genotoxic stress, patient cells harboured significantly more DNA damage than wild-type cells, as indicated by formation of longer comet tails (figure 1F). Although native patient fibroblasts did not show more DNA double-strand breaks, as demonstrated by costaining of phosphorylated histone H2AX (γH2AX) and p53-binding protein 1 (53BP1), they were more sensitive to ultraviolet (UV)-C-induced DNA double-strand breaks (figure 1G, see online supplementary figure S2), indicating that pre-existing DNA damage renders SAMHD1-deficient cells more vulnerable to genotoxic stress. We further compared genome-wide transcriptional profiles of native patient fibroblasts with wild-type cells (figure 2A). In agreement with the cellular phenotype of SAMHD1-deficient fibroblasts, we observed upregulation of genes involved in DNA damage signalling such as *CDKN1A* (p21) and *CDKN2A* (p16) (figure 2B) and in senescence-associated metabolic changes (see online supplementary figure S3). Conversely, genes functioning in de novo and salvage pathways of dNTP synthesis and in cell cycle progression were strongly downregulated (see online supplementary figure S3). Interestingly, transcriptional profiling of patient fibroblasts also revealed upregulation of genes involved in immune activation including several IFN-stimulated genes (figure 2C), which was validated by quantitative RT-PCR (see online supplementary figure S4). These findings suggest that

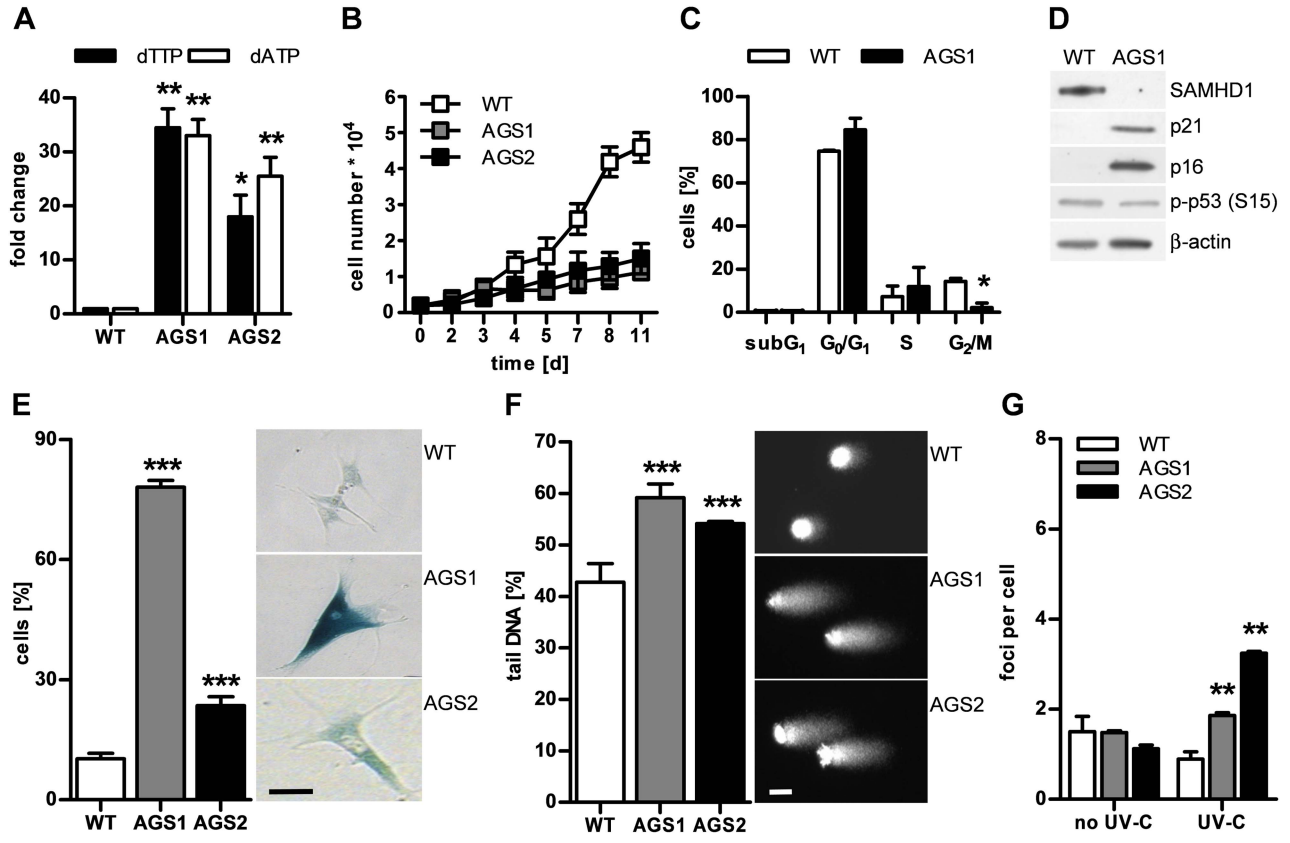

Figure 1 Dysregulation of deoxyribonucleoside triphosphate (dNTP) pools in SAMHD1-deficient fibroblasts causes genome instability leading to cell cycle delay and cellular senescence. (A, B) Fibroblasts from two patients with Aicardi–Goutières syndrome (AGS; AGS1, AGS2) exhibit markedly increased levels of deoxythymidine triphosphate (dTTP) and deoxyadenosine triphosphate (dATP) and proliferate more slowly than wild-type cells (WT, n=2). Shown are the means±SD of two independent experiments run in triplicate. (C) Synchronised AGS1 fibroblasts show delayed cell cycle progression, with an arrest in G_1 and S as well as (D) induction of the cell cycle inhibitors, p21 and p16, but not of p53 phosphorylated at S15. (E) Patient cells exhibit a senescent phenotype shown by a large increase in β-galactosidase-positive cells. Scale bar, 100 μm. (F) Alkaline single-cell gel electrophoresis reveals global DNA damage as shown by increased comet tail length and irregular nuclear contour in patient fibroblasts compared with wild-type cells. Scale bar, 10 μm. (G) Native patient cells do not show increased DNA double-strand breaks as determined by counting of γH2AX- and 53BP1-double positive nuclear foci, but are more susceptible to DNA double-strand breaks in response to low-dose ultraviolet (UV)-C (20 J/m^2). Values represent means±SEM of two (C, F, G) or three (D, E) independent experiments run in triplicate. *p<0.05, **p<0.01, ***p<0.001 vs wild-type by Student's t test.

constitutive low-level DNA damage or chronic activation of DNA damage signalling can cause innate immune activation.

SAMHD1 forms complexes with cyclin A in living cells

By affinity purification using GFP–SAMHD1 expressed in HEK293T cells as bait followed by MS analysis, we identified the cell cycle protein, cyclin A, as interactor. Cyclin A2 (GI:4502613) was confidently identified with two matching tryptic peptides: (R)EAGSALLALQQTALQEDQENINPEK and (R)AILVDWLVEVGEEYK (51 and 74 Mascot ion score, respectively). Interaction of SAMHD1 with cyclin A was validated by coimmunoprecipitation of cyclin A with GFP–SAMHD1 expressed in HEK293T cells. In addition, reverse coimmunoprecipitation of SAMHD1 using anti-cyclin A-coupled agarose beads confirmed interaction of SAMHD1 with cyclin A at the endogenous level (figure 3A, B). We also observed colocalisation of fluorescently tagged mCherry–SAMHD1 and GFP–cyclin A within the nucleus in HeLa cells (figure 3D). As SAMHD1 was shown to oligomerise,[17 19] we addressed complex formation of SAMHD1 with cyclin A in living HeLa cells by fluorescence cross-correlation spectroscopy, a confocal microscope-based technique that allows assessment of mobility properties as well as interactions of fluorescently labelled molecules in vitro and in living cells.[20] Cross-correlation between mCherry–SAMHD1 and GFP–cyclin A was 9.9±0.9% compared with 0.7±0.1% between monomeric GFP and mCherry, indicating formation of mobile complexes containing SAMHD1 and cyclin A within the nuclear environment (figure 3E). We further analysed the composition of these complexes by brightness analysis. The relative brightness of mCherry–SAMHD1 was on average twofold higher than monomeric mCherry, while that of GFP–cyclin A did not differ from monomeric GFP (figure 3E), suggesting that the formed complexes consisted on average of at least one cyclin A and two SAMHD1 molecules.

SAMHD1 is regulated by cyclin A in a cell cycle-dependent manner

Consistent with our proteomic data, which also identified CDK1 as a SAMHD1 interactor, CDK1 was pulled down by GFP–SAMHD1 along with cyclin A (figure 3A). Cyclin A regulates cell cycle progression in association with cyclin-dependent kinases by binding and phosphorylation of numerous target proteins. Analysis of mass spectra for phosphorylated SAMHD1 peptides revealed phosphorylation of threonine at position 592 (T592, see online supplementary figure S5), which is part of a bona fide consensus sequence for known CDK substrates

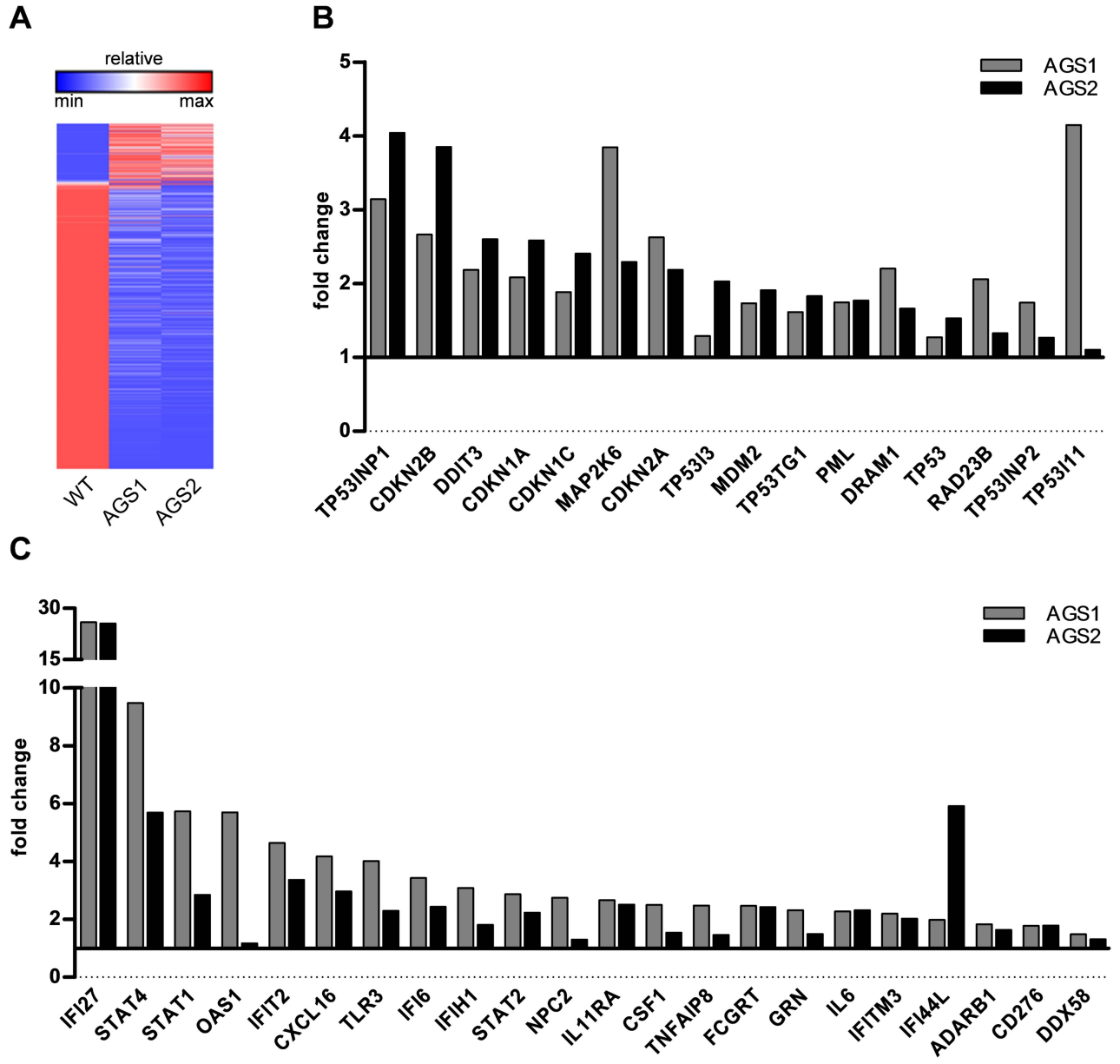

Figure 2 Genome-wide transcriptional profiles reveal upregulation of genes involved in DNA damage signalling and innate immune activation. (A) Heat maps based on RNA sequencing analysis represent hierarchically clustered transcripts showing up- or down-regulation by a factor of at least 2 in Aicardi–Goutières syndrome 1 (AGS1) and AGS2 compared with wild-type controls (WT, n=4). (B) Native patient fibroblasts exhibit constitutive upregulation of genes involved in the DNA damage response as well as (C) induction of interferon-stimulated genes. Indicated are the fold changes of the Reads Per Kilobase of exon per Million mapped reads (RPKM) values obtained by RNA sequencing analysis of patient fibroblasts (AGS1, AGS2) relative to the mean RPKM values of four WT cell lines.

((S/T*)PX(K/R), where S/T* is the phosphorylated serine or threonine and X any amino acid).[21] We further examined recombinant SAMHD1 by in vitro kinase assay using an antibody to phospho-T592-SAMHD1 and observed phosphorylation of SAMHD1 by cyclin A/CDK1, but not by cyclin A/CDK2 or cyclin E/CDK3 (figure 3C), confirming that SAMHD1 is phosphorylated by cyclin A/CDK1.

Since cyclin A level is tightly controlled during the cell cycle, we hypothesised that it may regulate SAMHD1 expression in a cell cycle-dependent manner. To investigate this further, we examined SAMHD1 expression in HeLa cells synchronised at G_0/G_1 by serum starvation. Cell cycle phases were monitored by immunoblotting analysis of additional cyclins as cell cycle markers and by flow cytometry (figure 3F and data not shown). After release of synchronised cells into growth medium, SAMHD1 protein was almost undetectable during G_1/S and gradually increased until late S phase (figure 3F). Corresponding to the course of SAMHD1 expression, dNTP levels were highest during G_1/S, reflecting a high demand for DNA precursors during genome replication, and decreased continuously until G_2/M (figure 3G). This was accompanied by the appearance of phosphorylated SAMHD1 paralleling cyclin A expression with a peak at G_2/M transition. SAMHD1 then disappeared at the beginning of the subsequent cell cycle (figure 3F). These findings are in agreement with variable SAMHD1 expression and phosphorylation observed in resting and cycling human fibroblasts and monocytic THP-1 cells.[22 23] Thus, SAMHD1 activity is subject to cell cycle-specific regulation at the post-translational level.

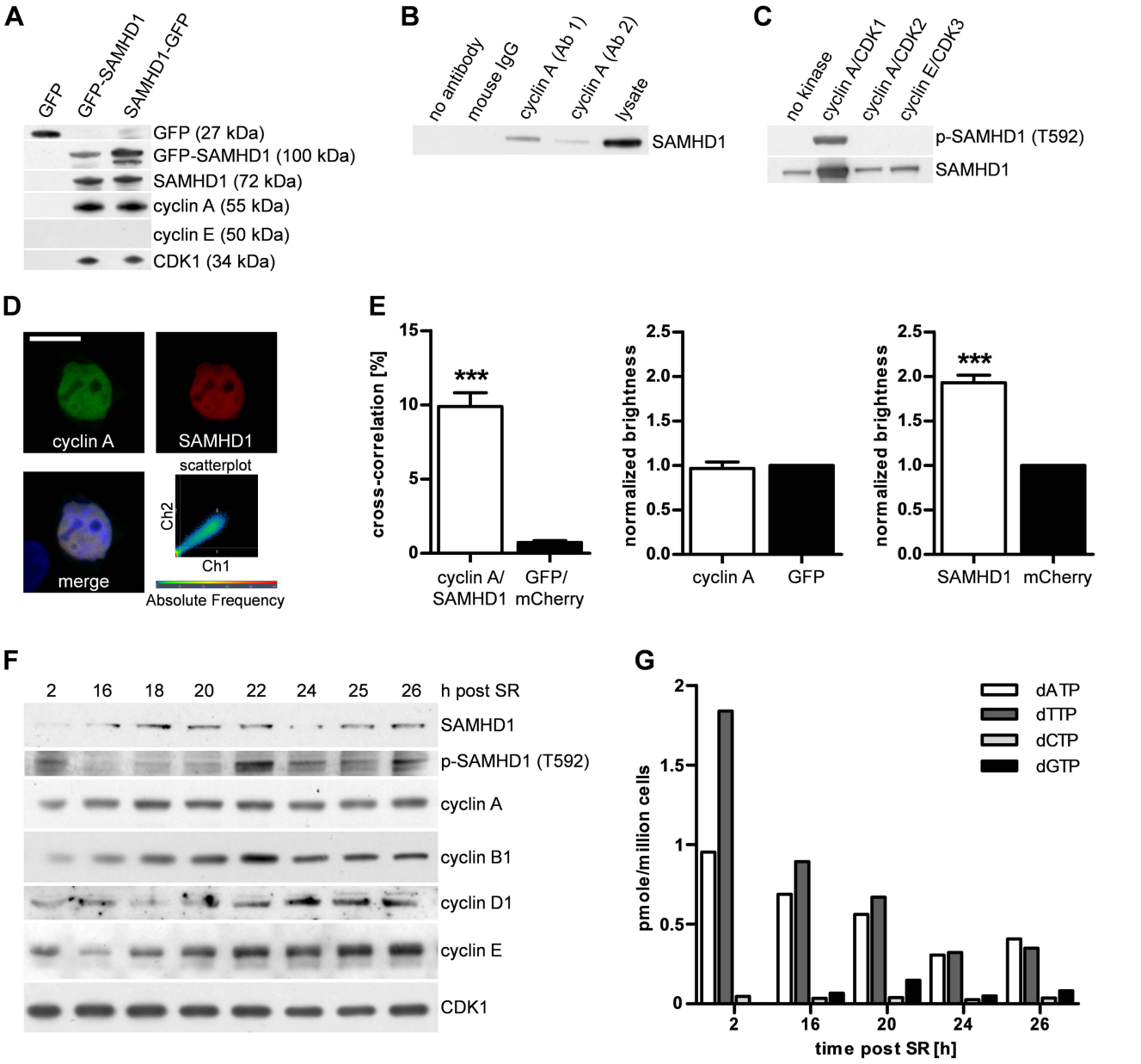

Figure 3 SAMHD1 is regulated by cyclin A in a cell cycle-specific manner. (A) Coimmunoprecipitation with N- or C-terminally green fluorescent protein (GFP)-tagged SAMHD1 expressed in HEK293T cells immobilised on GFP-Trap beads pulls down cyclin A and cyclin-dependent kinase 1 (CDK1), but not cyclin E. (B) Reverse coimmunoprecipitation with two different cyclin A antibodies (Ab 1, Ab 2) confirms interaction of SAMHD1 and cyclin A at the endogenous level. (C) In vitro kinase assay reveals phosphorylation of SAMHD1 at T592 by cyclin A/CDK1, but not by cyclin A/CDK2 or cyclin E/CDK3. (D) Cyclin A and SAMHD1 colocalise within the nucleus as shown by a high correlation of fluorescence signals in the scatter plot. Scale bar, 10 μm. (E) Fluorescence cross-correlation spectroscopy of living HeLa cells cotransfected with mCherry–SAMHD1 (SAMHD1) and GFP–cyclin A (cyclin A) shows a high cross-correlation, indicating formation of mobile SAMHD1–cyclin A complexes. Compared with monomeric GFP or mCherry, the average normalised brightness of GFP–cyclin A and mCherry–SAMHD1 is 1 or 2, respectively. At least 15 cells were measured per experiment. Data represent means±SEM from two independent experiments. ***p<0.001 by Student's t test. (F) HeLa cells synchronised at G_0/G_1 were lysed at the indicated time points after serum re-addition (SR) and immunoblotted with the indicated antibodies. (G) Intracellular deoxyribonucleoside triphosphate (dNTP) concentrations in HeLa cells treated as in (F).

SAMHD1 knockdown recapitulates the senescent phenotype and IFN activation

We next asked whether knockdown of SAMHD1 is sufficient to cause both activation of DNA damage signalling and type 1 IFN induction. Depletion of SAMHD1 in HeLa cells by RNA interference led to increased expression of p21 (figure 4A). This was accompanied by a delay in cell cycle progression and signs of cellular senescence, as shown by increased β-galactosidase activity (figure 4B,C). Furthermore, knockdown of SAMHD1 also led to transcriptional activation of *IFNB* and the IFN-stimulated genes, *IFI27*, *IFI6* and *DDX58* (figure 4D). Thus, depletion of SAMHD1 recapitulates the phenotypic changes observed in SAMHD1-deficient fibroblasts from patients with AGS.

DISCUSSION

We show that SAMHD1-deficient fibroblasts from patients with AGS exhibit increased dNTP pools and chronic DNA damage. Constitutive activation of DNA damage signalling results in

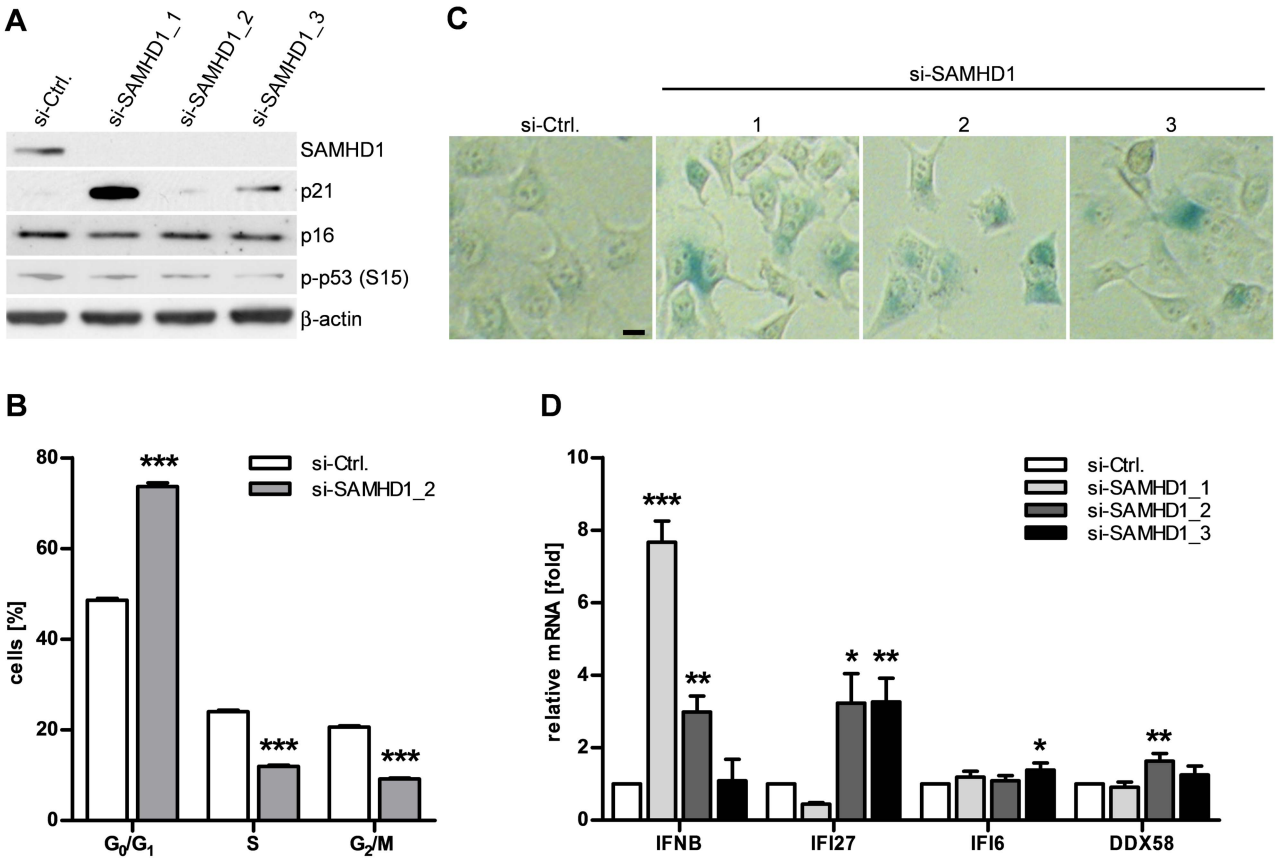

Figure 4 SAMHD1 knockdown recapitulates senescent phenotype and interferon (IFN) activation. (A) SAMHD1 is effectively knocked down in HeLa cells 72 h after transfection with SAMHD1-specific small interfering (si)RNAs (si-SAMHD1_1-3). Si-Ctrl, control-siRNA. This is accompanied by induction of p21. (B) Flow cytometry of propidium iodide-stained HeLa cells 72 h after transfection with si-SAMHD1_2 reveals delayed cell cycle progression and (C) an increase in β-galactosidase-positive cells. Scale bar, 10 μm. (D) SAMHD1 knockdown leads to induction of the *IFNB* gene and the interferon-stimulated genes *IFI27*, *IFI6* and *DDX58*. Gene expression was normalised to *GAPDH*. Shown is the relative fold change in gene expression relative to control siRNA. Data are represented as mean±SEM from three (A) or four (B, C, D) independent experiments run in triplicate. *p<0.05; **p<0.01; ***p<0.001 by Student's t test.

delayed cell cycle progression and cellular senescence. Senescence is a state of permanent cell cycle arrest and represents a cellular stress response that can be induced by various extrinsic and intrinsic stimuli including DNA damage.[24] Remarkably, complete deficiency of the AGS-causing nucleases, RNase H2 and TREX1, in mice is also associated with activation of DNA damage signalling.[25–27] This may suggest a common pathogenic mechanism in AGS involving DNA damage signalling. Furthermore, *Trex1*$^{-/-}$ mice exhibit increased lysosomal biogenesis,[28] a cellular phenotype that is typically observed during senescence,[24] raising the possibility that increased lysosomal activity may also contribute to AGS pathogenesis.

Transcriptional profiling of patient fibroblasts revealed induction of both genes of the DNA damage response as well as antiviral IFN-stimulated genes. Although upregulation of the *IFNB* gene was undetectable in patient fibroblasts, weak or intermittent type 1 IFN production cannot be excluded.[29] Chronic low-level accumulation of intracellular nucleic acids may not be sufficient to induce type 1 IFN greatly. Alternatively, upregulation of IFN-stimulated genes, but not of *IFNB*, may reflect the complex transcriptional regulation of IFN gene expression with multiple positive and negative regulatory elements.[30] Notably, the Irf3/STING/Tbk1-dependent activation of IFN-stimulated genes in *Trex1*$^{-/-}$ cells also occurs without detectable type 1 IFN induction.[28] However, constitutive activation of antiviral genes such as *STAT1* may prime IFN signalling and thereby enhance sensitivity to type 1 IFN stimuli.

dNTPs are the building blocks of DNA synthesis, and dNTP imbalances can have genotoxic consequences. Thus, changes in dNTP levels have been shown to impair replication fidelity, selection of replication origins, and fork progression.[31–33] The DNA precursor pool is tightly regulated by an intricate enzyme network orchestrating dNTP synthesis and degradation to ensure replication of the genome with high fidelity once per cell cycle. Expression of ribonucleotide reductase, which converts ribonucleotides into deoxyribonucleotides during de novo dNTP synthesis, and of thymidine kinase 1, responsible for salvage of deoxynucleosides, varies during the cell cycle and is highest during S phase when DNA synthesis takes place.[34] In agreement with previous reports,[23 35] we identified cyclin A as an SAMHD1 interactor. Moreover, we demonstrate formation of mobile SAMHD1–cyclin A complexes in living cells consisting of at least one cyclin A and two SAMHD1 molecules, suggesting that binding of cyclin A may either require or promote oligomerisation of SAMHD1. As SAMHD1 represents a major negative regulator of DNA precursor pools in mammalian cells,[22] our finding of cyclin A-dependent regulation of SAMHD1 provides a link between its dNTP-degrading activity and the cell cycle. Cyclin A is a key regulator of cell cycle progression and functions in association with cyclin-dependent kinases by phosphorylation

of numerous target proteins. While association of cyclin A with CDK2 is required for passage into S phase, cyclin A also associates with CDK1 in AS phase, and this complex persists into late G_2 phase, controlling the onset of mitosis.[36] SAMHD1 is phosphorylated by cyclin A/CDK1 and fluctuates during the cell cycle, with the lowest levels observed in S phase when genome duplication takes place. A gradual increase in SAMHD1 during late S phase coincides with the appearance of phosphorylated SAMHD1 at the G_2/M transition, which is followed by disappearance of SAMHD1. As phosphorylation of SAMHD1 by cyclin A/CDK1 does not interfere with catalytic activity,[23 35] our findings may suggest that cyclin A/CDK1-mediated phosphorylation may be involved in degradation of SAMHD1 during the cell cycle. This would enable the cell to further adapt its dNTP supply to the changing physiological demands throughout the cell cycle. Given that the lentiviral factor, Vpx, can mediate proteasomal degradation of SAMHD1 in a DCAF1/E3 ligase-dependent manner,[37] this raises the question of whether SAMHD1 may also be targeted for proteasomal degradation by as yet unknown physiological pathways.

The phenotype of AGS is characterised by inflammation and autoimmunity, which has been attributed to a type 1 IFN-mediated antiviral response induced by immune recognition of intracellular nucleic acids.[13] Although cancer has not been described in children with AGS thus far, increased sensitivity to genotoxic stimuli in patient cells suggests that SAMHD1 may have tumour-suppressive properties. This is supported by the recent finding of somatic SAMHD1 mutations in patients with chronic lymphatic leukaemia.[38 39] Patients with AGS are therefore predicted to have an increased cancer risk and should be closely monitored for malignant disease.

Our findings indicate that SAMHD1 maintains genome stability by regulating the DNA precursor pool, thereby preventing genotoxic dNTP imbalances. Loss of genome integrity in patient fibroblasts leads to upregulation of IFN-stimulated genes. Innate immune activation may be caused either by immune recognition of by-products of DNA repair or by as yet undefined signalling pathways of the DNA damage response. Since knockdown of SAMHD1 in HeLa cells is sufficient to recapitulate the phenotype of AGS patient fibroblasts, this supports a causal link between DNA damage signalling and innate immune activation. By limiting the dNTP supply available for DNA synthesis during replication and repair, SAMHD1 may also prevent aberrant synthesis of DNA species that could trigger a type 1-IFN-dependent immune response through activation of DNA sensors. Indeed, in *Trex1*$^{-/-}$ cells, type 1 IFN activation has been attributed to engagement of pattern-recognition receptors by cytosolic DNA, which may originate from DNA-repair processes or replication of endogenous retroviruses/retroelements.[40 41] As SAMHD1 has been shown to restrict HIV by limiting the dNTP pool required for reverse transcription of its RNA genome,[3] it may also restrict endogenous retroviruses/retroelements. This is supported by the recent finding that SAMHD1 can inhibit retrotransposition of a retroelement reporter in vitro.[42] However, the exact origin of the nucleic acid species mediating innate immune activation in SAMHD1 deficiency remains to be investigated.

Collectively, these findings implicate chronic DNA damage as a cell-intrinsic source of an IFN-dependent innate immune response. The ensuing constitutive IFN signalling could eventually promote initiation of autoimmunity. These findings link pathways involved in DNA damage signalling with activation of a type 1-IFN-dependent immune response in the pathogenesis of autoimmunity.

Author affiliations
[1]Department of Pediatrics, Medizinische Fakultät Carl Gustav Carus, Technische Universität Dresden, Dresden, Germany
[2]Biotechnology Center, Technische Universität Dresden, Dresden, Germany
[3]Cavendish Laboratory, Department of Physics, University of Cambridge, Cambridge, UK
[4]Department of Pediatrics, University Hospital, University of Aachen, Aachen, Germany
[5]Department of Pediatrics, Center for Drug Discovery, Emory University, Atlanta, Georgia, USA
[6]College of Pharmacy, Kyung-Hee University, Seoul, South Korea
[7]Center for Regenerative Therapies, Technische Universität Dresden, Dresden, Germany
[8]Department of Biology, Technische Universität Darmstadt, Germany
[9]Max Planck Institute of Molecular Cell Biology and Genetics, Dresden, Germany

Correction notice This article has been corrected since it was published Online First. The penultimate sentence of the Methods section of the Abstract has been amended.

Acknowledgements We thank Susan Hunger and Kerstin Engel for excellent technical assistance, Nicole Berndt for help with γH2AX/53BP1 immunofluorescence, Andrea Knaust for assistance in MS analysis, and Patrick Keller (Max Planck-Institute of Molecular Cell Biology and Genetics, Dresden, Germany) for generation of antibody to phospho-T592-SAMHD1. We thank Axel Roers, Rayk Behrendt, Victoria Tüngler and Claudia Günther for helpful discussion. MAL-K, JG and AS are members of the Clinical Research Group 249, Medical Faculty, TU Dresden.

Contributors SK, CW, NK, WS, HL, LAN, BK, DA, AD and AS performed experiments and analysed and interpreted data. MH, AR, MCC and JG provided material and advice. SK, AS and MAL-K conceived experiments, interpreted data and wrote the manuscript.

Funding This work was supported by the Deutsche Forschungsgemeinschaft (LE 1074/4-1 to MAL-K, GU 612/2-2 to JG, SH 569/1-1 to AS), the Bundesministerium für Bildung und Forschung (02S8355 and 02NUK017D to MCC), a grant from the Friede Springer Stiftung to MAL-K, and National Institutes of Health Grants AI077401 and AI049781 to BK.

Competing interests None.

Ethics approval Ethics Committee, Medical Faculty, TU Dresden.

Provenance and peer review Not commissioned; externally peer reviewed.

REFERENCES

1 Goldstone DC, Ennis-Adeniran V, Hedden JJ, *et al*. HIV-1 restriction factor SAMHD1 is a deoxynucleoside triphosphate triphosphohydrolase. *Nature* 2011;480:379–82.
2 Powell RD, Holland PJ, Hollis T, *et al*. Aicardi-Goutieres syndrome gene and HIV-1 restriction factor SAMHD1 is a dGTP-regulated deoxynucleotide triphosphohydrolase. *J Biol Chem* 2011;286:43596–600.
3 Lahouassa H, Daddacha W, Hofmann H, *et al*. SAMHD1 restricts the replication of human immunodeficiency virus type 1 by depleting the intracellular pool of deoxynucleoside triphosphates. *Nat Immunol* 2012;13:223–8.
4 Hrecka K, Hao C, Gierszewska M, *et al*. Vpx relieves inhibition of HIV-1 infection of macrophages mediated by the SAMHD1 protein. *Nature* 2011;474:658–61.
5 Laguette N, Sobhian B, Casartelli N, *et al*. SAMHD1 is the dendritic- and myeloid-cell-specific HIV-1 restriction factor counteracted by Vpx. *Nature* 2011;474:654–7.
6 Rice GI, Bond J, Asipu A, *et al*. Mutations involved in Aicardi-Goutieres syndrome implicate SAMHD1 as regulator of the innate immune response. *Nat Genet* 2009;41:829–32.
7 Ramantani G, Kohlhase J, Hertzberg C, *et al*. Expanding the phenotypic spectrum of lupus erythematosus in Aicardi-Goutieres syndrome. *Arthritis Rheum* 2010;62:1469–77.
8 Lebon P, Badoual J, Ponsot G, *et al*. Intrathecal synthesis of interferon-alpha in infants with progressive familial encephalopathy. *J Neurol Sci* 1988;84:201–8.
9 Marshak-Rothstein A. Toll-like receptors in systemic autoimmune disease. *Nat Rev Immunol* 2006;6:823–35.
10 Crow YJ, Leitch A, Hayward BE, *et al*. Mutations in genes encoding ribonuclease H2 subunits cause Aicardi-Goutieres syndrome and mimic congenital viral brain infection. *Nat Genet* 2006;38:910–16.
11 Crow YJ, Hayward BE, Parmar R, *et al*. Mutations in the gene encoding the 3′-5′ DNA exonuclease TREX1 cause Aicardi-Goutieres syndrome at the AGS1 locus. *Nat Genet* 2006;38:917–20.

12 Rice GI, Kasher PR, Forte GM, *et al*. Mutations in ADAR1 cause Aicardi-Goutieres syndrome associated with a type I interferon signature. *Nat Genet* 2012;44:1243–8.
13 Lee-Kirsch MA, Wolf C, Gunther C. Aicardi-Goutieres syndrome: a model disease for systemic autoimmunity. *Clin Exp Immunol* 2014;175:17–24.
14 Behrendt R, Schumann T, Gerbaulet A, *et al*. Mouse SAMHD1 has antiretroviral activity and suppresses a spontaneous cell-intrinsic antiviral response. *Cell Rep* 2013;4:689–96.
15 Rehwinkel J, Maelfait J, Bridgeman A, *et al*. SAMHD1-dependent retroviral control and escape in mice. *EMBO J* 2013;32:2454–62.
16 Mathews CK. DNA precursor metabolism and genomic stability. *FASEB J* 2006;20:1300–14.
17 Tungler V, Staroske W, Kind B, *et al*. Single-stranded nucleic acids promote SAMHD1 complex formation. *J Mol Med* 2013;91:759–70.
18 Kim B, Nguyen LA, Daddacha W, *et al*. Tight interplay among SAMHD1 protein level, cellular dNTP levels, and HIV-1 proviral DNA synthesis kinetics in human primary monocyte-derived macrophages. *J Biol Chem* 2012;287:21570–4.
19 Yan J, Kaur S, Delucia M, *et al*. Tetramerization of SAMHD1 is required for biological activity and inhibition of HIV infection. *J Biol Chem* 2013;288:10406–17.
20 Bacia K, Kim SA, Schwille P. Fluorescence cross-correlation spectroscopy in living cells. *Nat Methods* 2006;3:83–9.
21 Errico A, Deshmukh K, Tanaka Y, *et al*. Identification of substrates for cyclin dependent kinases. *Adv Enzyme Regul* 2010;50:375–99.
22 Franzolin E, Pontarin G, Rampazzo C, *et al*. The deoxynucleotide triphosphohydrolase SAMHD1 is a major regulator of DNA precursor pools in mammalian cells. *Proc Natl Acad Sci USA* 2013;110:14272–7.
23 White TE, Brandariz-Nunez A, Valle-Casuso JC, *et al*. The retroviral restriction ability of SAMHD1, but not its deoxynucleotide triphosphohydrolase activity, is regulated by phosphorylation. *Cell Host Microbe* 2013;13:441–51.
24 Campisi J, d'Adda di Fagagna F. Cellular senescence: when bad things happen to good cells. *Nat Rev Mol Cell Biol* 2007;8:729–40.
25 Yang YG, Lindahl T, Barnes DE. Trex1 exonuclease degrades ssDNA to prevent chronic checkpoint activation and autoimmune disease. *Cell* 2007;131:873–86.
26 Reijns MA, Rabe B, Rigby RE, *et al*. Enzymatic removal of ribonucleotides from DNA is essential for mammalian genome integrity and development. *Cell* 2012;149:1008–22.
27 Hiller B, Achleitner M, Glage S, *et al*. Mammalian RNase H2 removes ribonucleotides from DNA to maintain genome integrity. *J Exp Med* 2012;209:1419–26.
28 Hasan M, Koch J, Rakheja D, *et al*. Trex1 regulates lysosomal biogenesis and interferon-independent activation of antiviral genes. *Nat Immunol* 2013;14:61–71.
29 Taniguchi T, Takaoka A. A weak signal for strong responses: interferon-alpha/beta revisited. *Nat Rev Mol Cell Biol* 2001;2:378–86.
30 Honda K, Yanai H, Takaoka A, *et al*. Regulation of the type I IFN induction: a current view. *Int Immunol* 2005;17:1367–78.
31 Chabes A, Stillman B. Constitutively high dNTP concentration inhibits cell cycle progression and the DNA damage checkpoint in yeast Saccharomyces cerevisiae. *Proc Natl Acad Sci USA* 2007;104:1183–8.
32 Anglana M, Apiou F, Bensimon A, *et al*. Dynamics of DNA replication in mammalian somatic cells: nucleotide pool modulates origin choice and interorigin spacing. *Cell* 2003;114:385–94.
33 Poli J, Tsaponina O, Crabbe L, *et al*. dNTP pools determine fork progression and origin usage under replication stress. *EMBO J* 2012;31:883–94.
34 Rampazzo C, Miazzi C, Franzolin E, *et al*. Regulation by degradation, a cellular defense against deoxyribonucleotide pool imbalances. *Mutat Res* 2010;703:2–10.
35 Cribier A, Descours B, Valadao AL, *et al*. Phosphorylation of SAMHD1 by cyclin A2/CDK1 regulates its restriction activity toward HIV-1. *Cell Rep* 2013;3:1036–43.
36 Bloom J, Cross FR. Multiple levels of cyclin specificity in cell-cycle control. *Nat Rev Mol Cell Biol* 2007;8:149–60.
37 Schwefel D, Groom HC, Boucherit VC, *et al*. Structural basis of lentiviral subversion of a cellular protein degradation pathway. *Nature* 2014;505:234–8.
38 Wang L, Lawrence MS, Wan Y, *et al*. SF3B1 and other novel cancer genes in chronic lymphocytic leukemia. *N Engl J Med* 2011;365:2497–506.
39 Schuh A, Becq J, Humphray S,, *et al* Monitoring chronic lymphocytic leukemia progression by whole genome sequencing reveals heterogeneous clonal evolution patterns. *Blood* 2012;120:4191–6.
40 Stetson DB, Ko JS, Heidmann T, *et al*. Trex1 prevents cell-intrinsic initiation of autoimmunity. *Cell* 2008;134:587–98.
41 Yan N, Regalado-Magdos AD, Stiggelbout B, *et al*. The cytosolic exonuclease TREX1 inhibits the innate immune response to human immunodeficiency virus type 1. *Nat Immunol* 2010;11:1005–13.
42 Zhao K, Du J, Han X, *et al*. Modulation of LINE-1 and Alu/SVA Retrotransposition by Aicardi-Goutieres Syndrome-Related SAMHD1. *Cell Rep* 2013;4:1108–15.

SUPPLEMENTARY DATA

SAMHD1 prevents autoimmunity by maintaining genome stability

Stefanie Kretschmer[1], Christine Wolf[1], Nadja König[1], Wolfgang Staroske[2], Jochen Guck[2,3], Martin Häusler[4], Hella Luksch[1], Laura A. Nguyen[5], Baek Kim[5,6], Dimitra Alexopoulou[2,7], Andreas Dahl[2,7], Alexander Rapp[8], M. Cristina Cardoso[8], Anna Shevchenko[9], Min Ae Lee-Kirsch[1*]

[1] Department of Pediatrics, Medizinische Fakultät Carl Gustav Carus, Technische Universität Dresden, Dresden, Germany

[2] Biotechnology Center, Technische Universität Dresden, Dresden, Germany

[3] Cavendish Laboratory, Department of Physics, University of Cambridge, Cambridge, UK

[4] Department of Pediatrics, University Hospital, University of Aachen, Aachen, Germany

[5] Center for Drug Discovery, Department of Pediatrics, Emory University, Atlanta, Georgia USA

[6] College of Pharmacy, Kyung-Hee University, Seoul, South Korea

[7] Center for Regenerative Therapies, Technische Universität Dresden, Dresden, Germany

[8] Department of Biology, Technische Universität Darmstadt, Germany

[9] Max Planck Institute of Molecular Cell Biology and Genetics, Dresden, Germany

* Correspondence to:

Min Ae Lee-Kirsch, M.D.
Department of Pediatrics, Medizinische Fakultät Carl Gustav Carus
Technische Universität Dresden
Dresden, Germany
Fetscherstr. 74, 01307 Dresden, Germany
phone: +49-351-458 6878, fax: +49-351-458 6333
email: minae.lee-kirsch@uniklinikum-dresden.de

Supplementary methods

Immunoprecipitation, Western blot

Cells were lysed in RIPA buffer (50 mM Tris HCl, pH 7.4, 150 mM NaCl, 1 mM Na_2EDTA, 1 % Triton X-100, 1 mM Na_3VO_4 and 20 mM NaF) containing 2 U/ml DNase I (Invitrogen), protease and phosphatase inhibitors (Roche). Lysates were incubated with GFP-Trap_A beads (ChromoTek) or with anti-cyclin A-coupled agarose beads (abcam and BD Biosciences) and analyzed by Western blotting using the following antibodies: SAMHD1 (ProteinTech Group), CCNA and p21 (BD Biosciences), CCNB1, CCND1, CCNE, p16 and p-p53 (S15) (Santa Cruz), CDK1 (Cell Signaling), Alexa Fluor 594-phalloidin (Invitrogen), GFP (Roche) and β-actin (Sigma Aldrich). Anti-phospho-T592-SAMHD1-antibody was generated by immunization of mice with the phosphorylated peptide CAPLI(pT)PQKKE (aa 586-597). Immunoreactive signals were detected by chemiluminescence (Lumi-Light PLUS, Roche).

Mass spectrometry

GFP-SAMHD1 was purified on beads (GFP-Trap_A, ChromoTek) from transfected HEK293T cell lysates and separated by one-dimensional SDS-PAGE on a 4-12 % bis-Tris gel (NuPAGE; Invitrogen). After visualization with Coomassie staining the experimental lane was cut into 6-8 slices and each slice was separately in-gel digested with trypsin [1]. Retrieved tryptic peptides were analyzed by LC-MS/MS on an Ultimate3000 nanoLC systems (Dionex) interfaced on-line to an LTQ linear trap or LTQ Orbitrap XL hybrid mass spectrometer (Thermo Fisher Scientific) via the robotic nanoflow ion source TriVersaNanoMate (Advion BioSciences Ltd.) as described [2, 3]. Acquired MS/MS spectra were searched against Human IPI (July 2010) and full protein (NCBI, July 2011) databases using MASCOT software (Matrix Science, v.2.2.0) under the following settings: mass tolerance was ± 2 Da and ± 5 ppm for precursors for LTQ and LTQ Orbitrap XL, respectively, and ± 0.5 Da for fragments; variable modifications were propionamide (C), carbamidomethyl (C), and oxidation (M); and enzyme specificity was trypsin. Protein hits were evaluated using Scaffold software

(Proteome Software, v.3.1.4.1) under the following settings: minimal number of matched peptides - 2, peptide threshold – 95 %, protein threshold – 99 %. false discovery rate (FDR) calculated by Scaffold software was 0.1 % and 0.5 % for proteins and peptides, respectively.

Comet assay

Comet assays were performed using a modified version of the method described by Olive and Banath [4]. Frosted microscope slides (Fisher Scientific) were pre-coated with melted 0.5 % agarose (type II, Sigma) in PBS followed by 1 % agarose (type II, Sigma). 1.5 x 10^5 cells synchronized by 24 h serum starvation were suspended in 150 µl 1 % low-melting point agarose (type VII, Sigma) melted in PBS at 50 °C and dispersed on pre-warmed pre-coated slides. Experiments were run in triplicate for each experimental condition. After gelling, slides were incubated in alkaline lysis solution (2.5 M NaCl, 0.1 M EDTA, 10 mM Tris, 1% Triton X-100, pH 10) at 4 °C for 16-18 h. Slides were then washed 10 times for 10 min in PBS. Prior to electrophoresis, slides were equilibrated for 20 min in electrophoresis buffer. Electrophoresis was conducted in alkaline electrophoresis buffer (0.3 M NaOH, 1 mM Na2EDTA, pH 13) at 1 V/cm and 500 mA for 25 min. 200 µl Antifade with Sybr Gold (20 mM DABCO, 0.1 µl/ml Sybr Gold, 20 mM Tris-HCl, 80 % glycerol) was added to each slide and covered with cover slips. Microscopy was carried out at 10x magnification. Images were captured using constant exposure times and 20 cells per slide were analyzed using CASP (CASPLab). The fluorescence intensity of the comet tail relative to the head reflects the number of DNA breaks.

Confocal microscopy, immunofluorescence and UVC irradiation

Cells were grown on glass cover slips in 24-well cell culture plates. For co-localization analysis, HEK293T cells were co-transfected with GFP-cyclin A and mCherry-SAMHD1 using polyethylenimine, fixed with 4 % paraformaldehyde, mounted with VectaShield containing DAPI and analyzed by confocal microscopy. For staining of DNA double-strand breaks,

fibroblasts were fixed with 4 % paraformaldehyde, permeabilized with 0.5 % Triton-X-100 in PBS and probed with mouse-anti-γH2AX (Ser-139; clone 2F3; Novus Biologicals) and rabbit-anti-53BP1 (Novus Biologicals). Slides were then probed with Alexa Fluor 546-conjugated goat-anti-mouse-IgG and Alexa Fluor 488-conjugated goat-anti-rabbit-IgG (Molecular Probes), respectively, mounted in VectaShield Mounting Medium containing DAPI (Vector Labs). γH2AX/53BP1 double positive nuclear foci were counted in at least 30 cells per slide. Fibroblasts were irradiated with UVC (20 J/m^2) and incubated for 6 h prior to staining. Fluorescence images were captured using a LSM510 confocal microscope (Zeiss). The scatter plot was created with ZEN2012 (Zeiss).

RNA sequencing

For RNA sequencing mRNA was enriched from 2 µg total RNA using magnetic poly-dT bead based separation (Illumina). Strand-specific RNA sequencing libraries were prepared using the TruSeq Stranded mRNA Sample Prep Kit (Illumina). Libraries were checked for integrity by capillary electrophoresis (Fragment Analyzer, Advanced Analytical) and quantified by qPCR using the KAPA Library Quantification Kit (KAPA Biosystems). Equimolar amounts of barcoded libraries were pooled and sequenced using the HiSeq 2000 system (Illumina). On average 41 million 75 bp single end reads were generated for each sample with an average mappability of 90 %. For data analyses a splice junction library with a length of 120 nucleotides (60 + 60) per splice junction was created based on known exon-exon junctions according to the Ensembl Genes annotation (v. 67, May 2012) [5]. Alignment of the reads to the hg19 transcriptome was performed with pBWA [6]. A counts-per-gene table was created based on the overlap of the uniquely mapped reads with the Ensembl Genes annotation for hg19, using BEDtools (v. 2.11) [7]. RPKM (reads per kilobase per million reads) values were calculated based on the raw read counts and used as a measure of absolute expression levels. Heat maps were constructed using GENE-E (Broad Institute) [8].

Fluorescence cross-correlation spectroscopy

In dual color FCCS, the excitation of two spectrally different dyes in the same detection volume allows measuring the interactions between differently labeled molecules [9]. Two superimposed laser lines of different wavelength are focused by a single microscope objective in order to generate overlapping focal volume elements. In this way, two spectrally distinct dyes can be simultaneously excited and their fluorescence emission detected via the same objective in two separate channels. In fluid environments, diffusion of fluorescent molecules through the focal spot induces fluorescence fluctuation. Both fluctuating fluorescence signals are subjected to auto-correlation analysis. Additionally, the calculated cross-correlation function is obtained by correlating intensity fluctuations of both channels with each other. Only when a dual labeled molecule translocates through the detection volume it contributes to the cross-correlation curve. Hence, the amplitude of the cross-correlation curve is directly proportional to the amount of double labeled species and allows a quantitative analysis of interactions.

1.5×10^4 HeLa cells were grown in fibronectin-coated 8-well chamber slides and transfected with 22 ng of GFP-cyclin A and 7.5 ng of mCherry-SAMHD1, respectively, using FuGene HD (Roche Diagnostics). FCCS was carried out on a commercial system consisting of a LSM780 and a ConfoCor3 (Zeiss). The 488 nm and 561 nm laser lines were attenuated by an acousto-optical tunable filter and directed via a 488/561 dichroic mirror onto the back aperture of a Zeiss C-Apochromat 40x, N.A. = 1.2, water immersion objective. The laser intensity in the focal plane was 0.67 kW/cm² (GFP) or 1.34 kW/cm² (mCherry), respectively. Fluorescence emission light was collected by the same objective and split into two spectral channels by a second dichroic (LP565). To remove any residual laser light, a 495-555 nm bandpass and 580 nm longpass emission filter, respectively, were employed. The fluorescence was recorded by avalanche photodiode detectors (APDs) in each channel. Out-of-plane fluorescence was rejected with a 35 µm pinhole. The fluorescence signals were software-correlated by ZEN software (Zeiss) and evaluated with MATLAB (Mathworks) by using weighted Marquardt nonlinear least-square fitting routine. For brightness analysis,

correction of the measured brightness of mCherry particles containing a dark fraction was carried out as previously described [10].

Supplementary references

1 Shevchenko A, Tomas H, Havlis J, Olsen JV, Mann M. In-gel digestion for mass spectrometric characterization of proteins and proteomes. Nat Protoc 2006;1:2856-60.

2 Shevchenko A, Roguev A, Schaft D, Buchanan L, Habermann B, Sakalar C, et al. Chromatin Central: towards the comparative proteome by accurate mapping of the yeast proteomic environment. Genome Biol 2008;9:R167.

3 Junqueira M, Spirin V, Santana BT, Waridel P, Surendranath V, Kryukov G, et al. Separating the wheat from the chaff: unbiased filtering of background tandem mass spectra improves protein identification. J Proteome Res 2008;7:3382-95.

4 Olive PL, Banath JP. The comet assay: a method to measure DNA damage in individual cells. Nat Protoc 2006;1:23-9.

5 Flicek P, Amode MR, Barrell D, Beal K, Brent S, Chen Y, et al. Ensembl 2011. Nucleic Acids Res 2011;39:D800-D806.

6 Li H, Durbin R. Fast and accurate long-read alignment with Burrows-Wheeler transform. Bioinformatics 2010;26:589-95.

7 Quinlan AR, Hall IM. BEDTools: a flexible suite of utilities for comparing genomic features. Bioinformatics 2010;26:841-2.

8 Subramanian A, Tamayo P, Mootha VK, Mukherjee S, Ebert BL, Gillette MA, et al. Gene set enrichment analysis: a knowledge-based approach for interpreting genome-wide expression profiles. Proc Natl Acad Sci U S A 2005;102:15545-50.

9 Bacia K, Kim SA, Schwille P. Fluorescence cross-correlation spectroscopy in living cells. Nat Methods 2006;3:83-9.

10 Tungler V, Staroske W, Kind B, Dobrick M, Kretschmer S, Schmidt F, et al. Single-stranded nucleic acids promote SAMHD1 complex formation. J Mol Med 2013;91:759-70.

Supplementary table 1. Sequences of SAMHD1-siRNAs. All siRNAs including the control siRNA (Negative Control #1 siRNA) were purchased from Ambion.

name	sense (5´-3´)	antisense (5´-3´)
si-SAMHD1_1	GCAGAUAAGUGAACGAGAUtt	AUCUCGUUCACUUAUCUGCag
si-SAMHD1_2	GUAUCGCAUUUCUACAGCAtt	UGCUGUAGAAAUGCGAUACtt
si-SAMHD1_3	CGCAACUCUUUACACCGUAtt	UACGGUGUAAAGAGUUGCGag

Supplementary table 2. Oligonucleotides used for quantitative RT-PCR. Oligonucleotides were purchased from Eurofins MWG Operon. IFI6 gene expression was determined using a pre-designed TaqMan Gene Expression Assay (Applied Biosystems).

name	**sequence (5´-3´)**
IFNB_F	ACCTCCGAAACTGAAGATCTCCTA
IFNB_R	TGCTGGTTGAAGAATGCTTGA
IFNB_P	FAM-CCTGTGCCTCTGGGACTGGACAATTG-TAMRA
IFI44_F	TCTATTCAATACTTCTCCTCTCAGATGATAG
IFI44_R	TGAGCAAAGCCACATGTACCA
IFI44_P	FAM-CCAGCGTTTACCAACTCCCTTCGAATTCTT-TAMRA
IFI27_F	AGCAGTGACCAGTGTGGCCAAAGT
IFI27_R	CTCCAATCACAACTGTAGCAATCC
IFI27_P	FAM-CCTCTGGCTCTGCCGTAGTTTTGCC-TAMRA
DDX58_F	AAAGCCTTGGCATGTTACACA
DDX58_R	TGGTCTACTCACAAAGCATTCCT
DDX58_P	FAM-AAGCATCTCCAAGCACAGTGTAATGGCA-TAMRA
GAPDH_F	GAAGGTGAAGGTCGGAGTC
GAPDH_R	GAAGATGGTGATGGGATTTC
GAPDH_P	FAM-CAAGCTTCCCGTTCTCAGCC-TAMRA

Supplementary figure 1. Senescence-associated morphological changes in SAMHD1-deficient fibroblasts. Formation of senescence-associated heterochromatin foci (SAHF, arrows) indicating chromatin silencing in AGS1. Irregular and enlarged morphology of patient cells shown by staining with the cytoskeleton marker phalloidin. Scale bar, 10 µm.

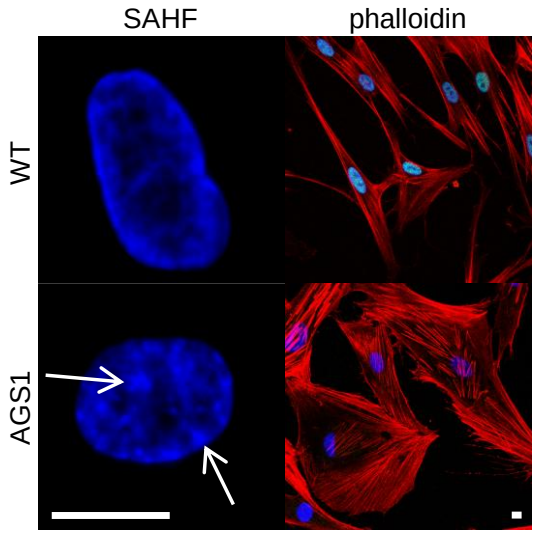

Supplementary figure 2. Immunofluorescence staining of DNA double-strand breaks in AGS patient fibroblasts. DNA double-strand breaks (DSBs) were visualized by co-staining for γH2AX (red) and 53BP1 (green) in native fibroblasts and 6 h after irradiation with low dose UV-C (20 J/m²). DSBs appear as double positive foci. Nuclei were counterstained with DAPI (blue). Shown are representative images from two independent experiments.

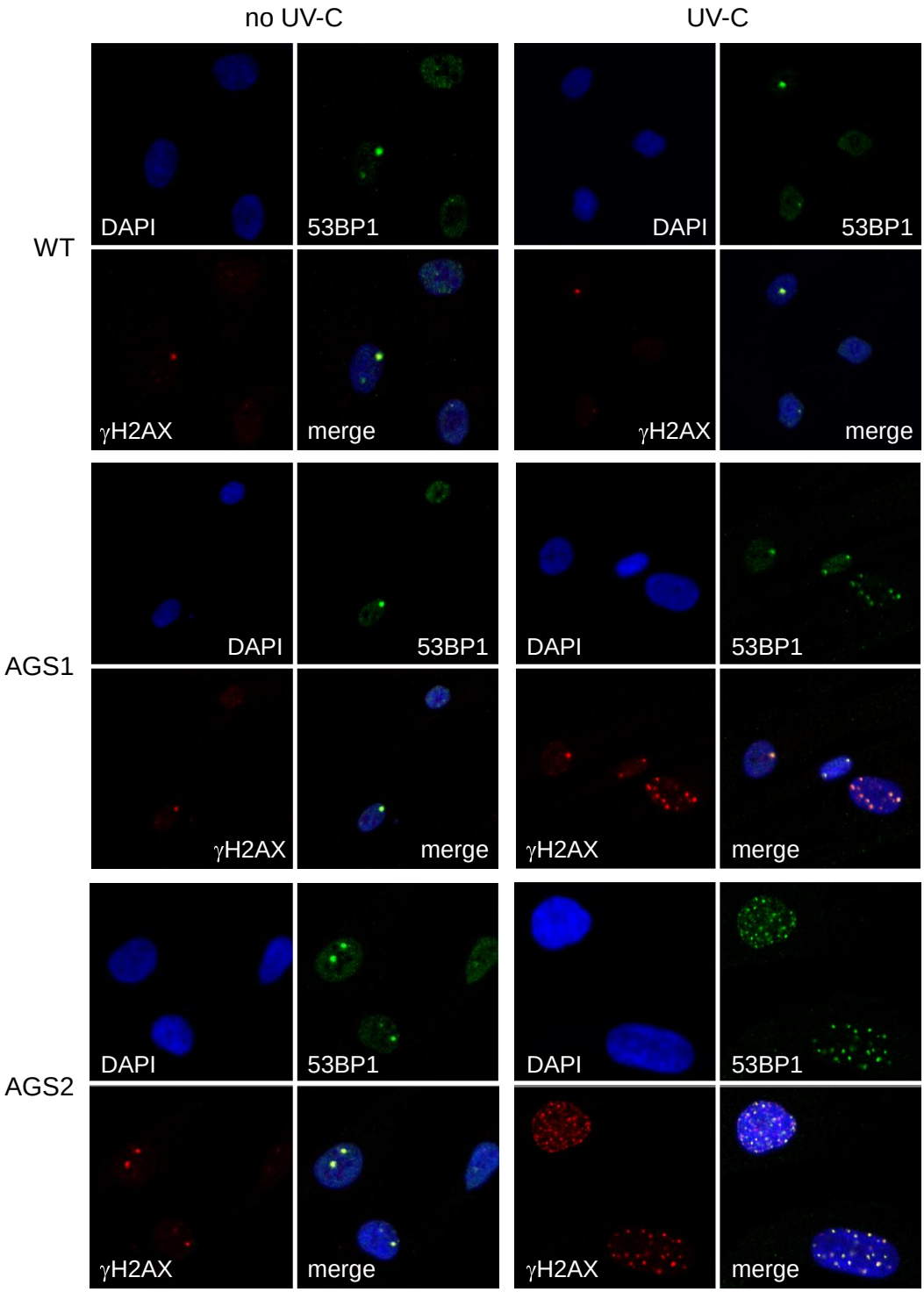

Supplementary figure 3. Expression of selected genes from transcriptome analysis. Shown are gene networks involved in dNTP synthesis (**A**), senescence-associated metabolic changes (**B**) and cell cycle progression (**C**). Indicated are the fold-changes of the RPKM values obtained by RNA sequencing analysis of patient fibroblasts (AGS1, AGS2) relative to the mean RPKM values of 4 wild type (WT) cell lines.

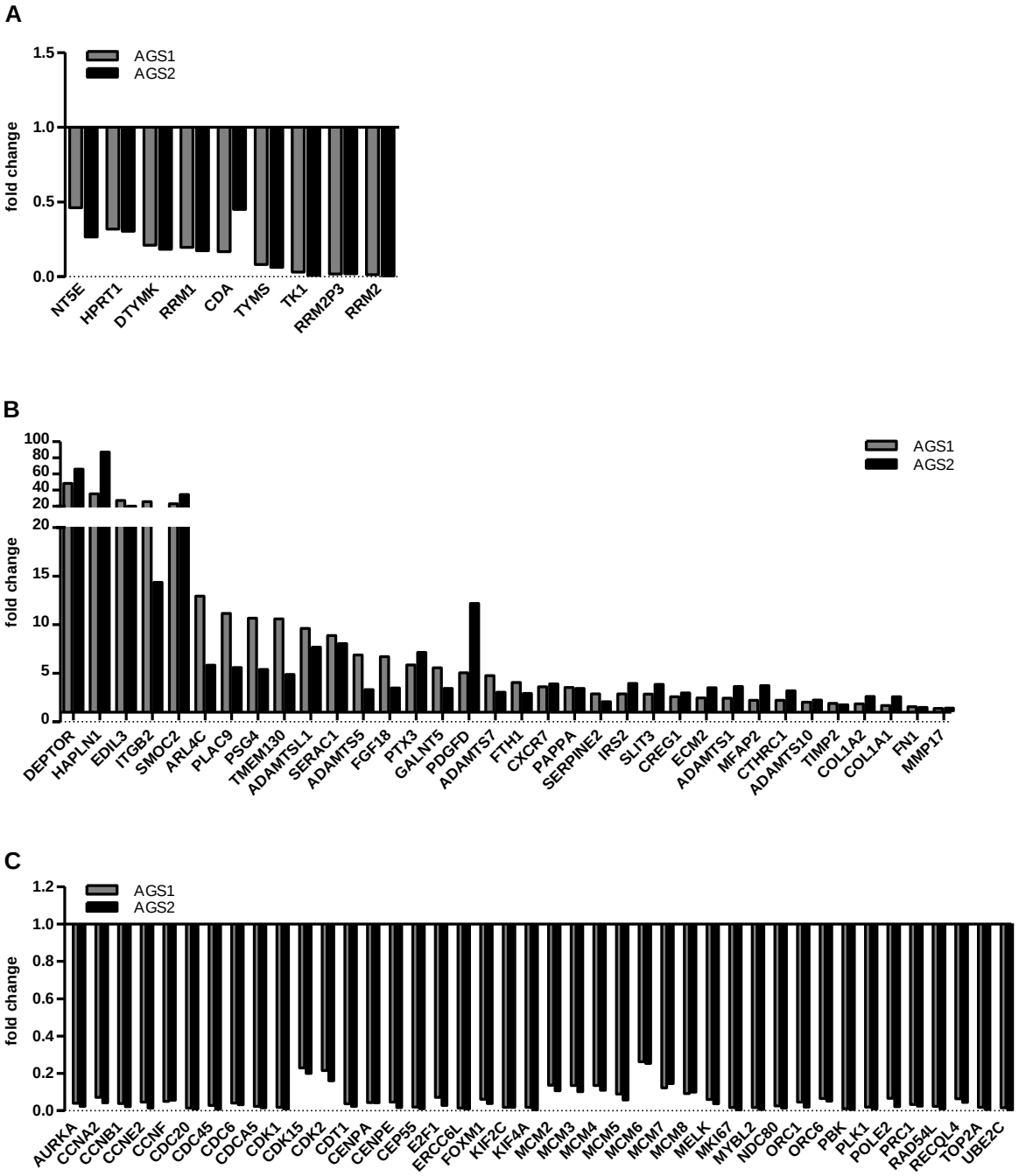

Supplementary figure 4. Validation of gene expression of selected IFN-stimulated genes in AGS fibroblasts. Gene expression of *IFNB*, *IFI27*, *IFI6*, *IFI44* and *DDX58* was determined by quantitative RT-PCR in fibroblasts of AGS patients (AGS1 and AGS2) and wild type control cells (WT). Indicated is the fold-change in gene expression relative to control. Gene expression was normalized to *GAPDH*. Data are represented as mean ± SEM of three technical replicates. ***: $P < 0.001$ by Student´s t test.

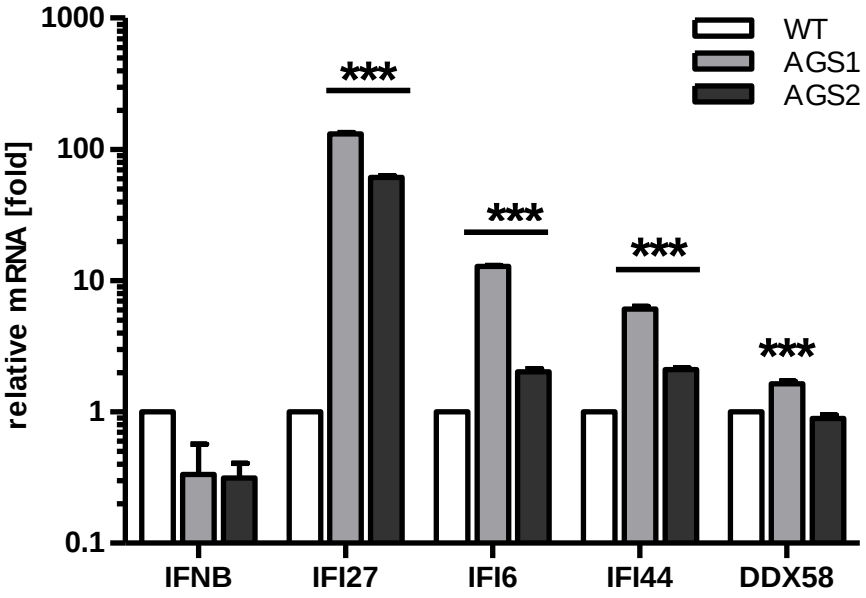

Supplementary figure 5. Mass spectrometry data showing phosphorylated SAMHD1. Mass spectrometric analysis of SAMHD1 digestion mixture detected two tryptic and three semi-tryptic peptides comprising phosphorylated threonine at position 592 (T592). The fragmentation spectrum of the doubly charged precursor ion with m/z 1081.552 which was confidently matched to the phosphorylated tryptic peptide sequence NFTKPQDGDVIAPLITpPQK is presented. The inset shows the low mass region of the spectrum with the phosphor-group at the T592 position.